Chemical Engineering Journal 479 (2024) 147655

Contents lists available at ScienceDirect

Chemical Engineering Journal

journal homepage: www.elsevier.com/locate/cej

Metal-organic frameworks for efficient mephedrone detoxification or supervised withdrawal – synthesis, characterisation, and *in vivo* studies

Kornelia Hyjek [a], Grzegorz Kurowski [a], Klaudia Dymek [a], Anna Boguszewska-Czubara [b], Barbara Budzyńska [c], Olga Wronikowska-Denysiuk [c], Aleksandra Gajda [d], Witold Piskorz [e], Paweł Śliwa [a], Magdalena Szumera [f], Piotr Jeleń [f], Maciej Sitarz [f], Przemysław J. Jodłowski [a,*]

[a] Faculty of Chemical Engineering and Technology, Cracow University of Technology, 24 Warszawska, 31-155 Kraków, Poland
[b] Department of Medical Chemistry, 4A Chodzki, Medical University of Lublin, 20-093 Lublin, Poland
[c] Independent Laboratory of Behavioral Studies, 4A Chodzki, Medical University of Lublin, 20-093 Lublin, Poland
[d] Strata Mechanics Research Institute of the Polish Academy of Sciences, Reymonta 27, 30-059 Kraków, Poland
[e] Faculty of Chemistry, Jagiellonian University, Gronostajowa 2, 30-387 Kraków, Poland
[f] Faculty of Materials Science and Ceramics, AGH University of Krakow, Mickiewicza 30, 30-059 Kraków, Poland

ARTICLE INFO

Keywords:
Mephedrone
Detoxication
Metal–organic frameworks
Cardiotoxicity
Locomotor activity
DFT
MD

ABSTRACT

In this study, we describe the innovative use of metal–organic frameworks (MOFs) as propranolol (PRO) carriers for mephedrone (4-MMC) overdose treatment or supervised withdrawal. The group of model Zr-based MOFs including UiO-66, UiO-67, MOF-808, and NU-1000, and PRO@MOF composites were synthesised and characterised. The PRO release was tested in water and simulated body fluid (SBF) environments. The prepared PRO@MOF differed in the amount and pore sizes, as well as in the surface properties, which affected the kinetics of PRO release. The inhibitory effect of SBF resulted in a more gradual, and controlled PRO release from PRO@MOF composites, further confirming the feasibility of this type of solution in real applications. The sorption mechanism in prepared PRO@MOF composites was studied by molecular dynamics (MD) and density functional theory (DFT) calculations. The molecular calculations (ring orientation, partial charges and bond orders) confirmed π–π stacking as the main contribution to the interaction between the electronic structures of PRO molecule and MOFs linker. The *in vivo* studies demonstrated the lack of cytotoxicity of MOFs and composites, and pre-evidence confirmed the effectiveness of using PRO-loaded MOFs as drug carriers in a 4-MMC overdose. The study provides a new potential detoxification system for addicts.

1. Introduction

Synthetic cathinones (SCs), classified as new psychoactive substances (NPS), exhibit effects closely resembling the pharmaceutical properties of amphetamine and amphetamine-like compounds [1]. These substances, otherwise known as "legal highs", "designer drugs" or "bath salts", are becoming increasingly popular, and thus easily accessible and widespread [2,3]. The European Monitoring Centre for Drugs and Drug Addiction (EMCDDA [4]) has monitored more than 670 new NPs available (data from the end of 2017) of which SCs were the most numerous group of all seizures. The characteristic feature of SCs is their structural similarity to (±)-cathinone. The most common compound included in this group is 4-methylmethcathinone (4-MMC, mephedrone, β-ketoamphetamine). This was first synthesised by Sanchez in 1929 [5]. Despite its short-acting time, 4-MMC causes euphoria and empathy, and increases libido and feelings of arousal. The United States, Germany and Sweden, among others, made 4-MMC illegal in 2010. Nowadays, the 4-MMC is treated as an illegal psychoactive substance in the vast majority of countries. However, due to its widespread presence and low price, it is one of the most commonly abused drugs among young people [5].

Recently, it has been noted that β-adrenergic receptor antagonists (β-blockers) can interact in combination with psychoactive compounds, causing a reduction in the side effects of their use. β-blockers are commonly used to lower blood pressure and protect against cardiac arrhythmias [6]. β-blockers, such as propranolol (PRO, (±)-1-isopropylamino-3-(1-naphthyloxy)-2-propanol), may be used in the treatment of amphetamine intoxication. They act by blocking the effects of norepinephrine and decreasing heart rate, blood pressure, and agitation.

* Corresponding author.
E-mail address: przemyslaw.jodlowski@pk.edu.pl (P.J. Jodłowski).

https://doi.org/10.1016/j.cej.2023.147655
Received 27 July 2023; Received in revised form 30 October 2023; Accepted 23 November 2023
Available online 28 November 2023

β-blockers, in an amphetamine overdose, are typically used in combination with other treatments such as benzodiazepines and supportive care [2]. PRO is a non-selective β-adrenergic receptor antagonist. This small molecule counteracts vasoconstriction, slows down the work of the heart muscle, and exhibits antiarrhythmic effects. Considering the negative effects of 4-MMC, more specifically, cardiovascular symptoms such as tachycardia, palpitations, hypertension, and myocarditis, PRO can be successfully used in the event of 4-MMC overdose or supervised withdrawal treatment. Moreover, PRO is readily available and inexpensive, which is conducive to scientific research in this area [2,7–9].

Although there are justifiable reasons for delivering PRO in the case of an overdose of SCs, safe and controlled delivery routes of this β-blocker are in high demand. Of the many drug delivery systems, the use of metal–organic frameworks (MOFs) appear to be the most optimal and prospective solution [10,11]. MOFs belong to the group of porous materials with well-defined structures and are distinguished by high biocompatibility, bioavailability and relatively high drug loadings [12]. Many examples of the applications of MOFs as efficient drug carriers have recently been described in the literature [13–18]. Experimental studies have demonstrated the successful use of MOFs as drug delivery systems (DDS) for many types of drugs including dichloroacetone (DCA) [19,20], 5-fluorouracil (5-FU) [21–23], α-cyano-4-hydroxycinnamic acid (α-CHC) [24,25], doxorubicin (DOX) [26–29], oxaliplatin [11], and many others. Among numerous MOF structures, zirconium-based MOFs are of high interest to researchers due to their unique properties such as ease of synthesis, high chemical and thermal stability, high stability in different media (acids, water, and water vapour), and ease of modification of sorption parameters through post-synthesis treatment. The model group of UiO-66, UiO-67, MOF-808, and NU-1000 is also reported to be potentially safe for living organisms, showing no substantial cytotoxicity of linkers or metal ions building MOF structure [30,31]. In our previous work, zirconium-based MOFs (UiO-66, UiO-67, MOF-808, and NU-1000) were used as acriflavine carriers against SARS-CoV-2 virus [32]. Furthermore, the *in vivo* and *in vitro* experiments have proven their low cellular cytotoxicity, cardioprotective effects, and prolonged drug delivery while minimising side effects [11,32].

Considering the constantly growing problem of psychoactive substance abuse and the easy access to SCs, including 4-MMC, one aim of our research was to highlight the prospective use of Zr-based MOFs as PRO hydrochloride carriers for 4-MMC detoxification or supervised withdrawal. Encouraged by the success in the effective adsorption of 4-MMC over UiO-66 and NU-1000 in our previous study [33], we would like in this paper (being somewhat a continuation of our previous studies) to expand the idea of the application of Zr-based MOFs as an efficient PRO carrier. In all adsorbates we have studied, the π-π stacking mechanism was responsible for the binding energy wherever the sorption was observed. In the literature describing the use of MOFs as a potential drug carrier, a great many possible drugs were recently reported. In our recent review devoted to the application of MOFs as drug carriers and adsorbents [34], we describe the most popular drugs and the MOFs used. It may be noted that the differences in chemical structure, or electronic properties, require an individual approach for the determination of the possibility of drug dosage through MOFs. As previously reported for UiO-66 family MOFs, their adsorption properties are influenced not only by their structural properties but also by the local electronic changes implied by the incorporation of functional groups (e.g., $–NH_2$, –COOH, $–SO_3H$). The adsorption/desorption efficiency is thus a derivative of the structural and electronic properties of the MOF serving as a drug carrier, and by the mutual interactions between the MOF framework and the incorporated drug. Since the number of possible interactions between guest and host molecules is at least limited by the number of possible MOFs and drugs, the mutual interactions between MOF and drug should be considered for each system separately. Since the Zr-MOFs are still under intense investigation and the number of proposed drugs that were previously considered is still limited, the mutual interactions between drug and MOF by experimental and molecular approaches are of great interest.

Although the possibility of the use of Zr-MOFs as an efficient adsorbent of toxic substances is widely reported in the literature, to our best knowledge, the use of PRO@MOF composites for efficient mephedrone detoxification and withdrawal has not yet been reported. The nature of PRO action is to inhibit angiogenic factors and vasoconstriction [7,35]. It has been noted that this action is opposite to that induced by SCs, including 4-MMC. Ingestion of 4-MMC is usually associated with cardiac arrhythmia and increased blood pressure [36,37]. Given the opposing action profiles of PRO and 4-MMC, the use of the drugs which are β-adrenergic receptor antagonists may limit the effects of 4-MMC overdose [7,9]. In addition, PRO can relieve 4-MMC withdrawal symptoms such as drowsiness, anhedonia, and irritability. The structures of both PRO and 4-MMC are shown in Fig. 1.

Thus, in this study, an innovative and prospective method of PRO administration in an acute overdose or supervised withdrawal is proposed. We want to answer the following questions: a) is it possible to use zirconium-based MOFs as a delivery system for PRO hydrochloride? b) can PRO@MOF composites be used as an innovative detoxification system in SCs overdose? c) how will PRO@MOF composites affect living organisms?

To answer the above-posed questions comprehensively, we describe in this paper a step-by-step approach to the development of Zr-MOFs and PRO@MOF composites, the release profiles of the drug into different media, and *in vitro* and *in vivo* studies. The research on the sorption and controlled release of PRO from the MOF structure was complemented by classical molecular dynamics (MD) and density functional theory (DFT) calculations.

2. Experimental

2.1. Material synthesis and characterisation

A series of zirconium-based metal–organic frameworks (MOFs), commonly known as UiO-66 [32], UiO-67 [38], MOF-808 [39], and NU-1000 [40], was synthesised based on procedures available in the literature [32]. Specific information on the synthesis of pristine MOF samples is provided in the Supporting Information file.

The synthesised materials were characterised using powder X-ray diffraction (PXRD), low-temperature N_2 adsorption (BET), Fourier Transform Infrared Spectroscopy (FTIR), Scanning Electron Microscopy (SEM), and μRaman spectroscopy. A detailed description of characterisation methods is available in the Supporting Information file.

To characterise PRO@MOF composites, a computational approach using density functional theory (DFT) and molecular dynamics (MD) was applied. A detailed description of the methodology and models used are provided in the Supporting Information file.

2.2. Propranolol@MOF composites (PRO@MOF)

PRO@MOF composites were synthesised as described below. In brief, 100 mg of activated MOF (UiO-66, UiO-67, MOF-808, NU-1000) was heated in Schlenk tubes at 120 °C under vacuum for 1 h. At the same time, 100 mg of PRO hydrochloride was dissolved in 10 mL of distilled water. The solution of PRO in water was then injected into the heated MOFs. The whole mixture was stirred for 24 h, followed by separation by centrifugation (10 min, 6000 rpm). The resulting composites were called PRO@UiO-66, PRO@UiO-67, PRO@MOF-808, and PRO@NU-1000, respectively. The filtrates were used to calculate the percentage of drug loading.

The amount of PRO loaded in PRO@MOF composites was calculated from the filtrates of PRO hydrochloride solution after the PRO loading into the PRO@MOF composites by using UV–Vis spectroscopy (AvaSpec-ULS3648 high-resolution spectrometer, deuterium-halogen light source AvaLight-DHc and Sarspec CH-MP cuvette holder) by monitoring the maximum absorbance at 290 nm. From each PRO filtrate, the 10 mL

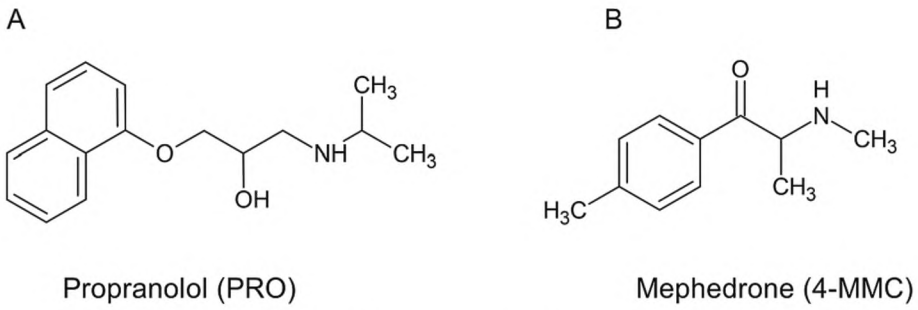

Fig. 1. **(A)** Propranolol (PRO) structure; **(B)** Mephedrone structure (4-MMC).

of PRO hydrochloride solution was collected and diluted with distilled water and the resulting UV–Vis spectrum was collected. The amount of PRO@MOF was determined from calibration curves prepared for H_2O and SBF solution (see Supporting Information file, Figure S2).

The amount of the PRO loading in prepared PRO@MOF composites was determined using the following formula:

$$\text{Propranolol } (wt.\,\%) = \left[\frac{m\text{PRO} - C{\cdot}10\,\text{mL}}{m\text{MOF} + m\text{PRO} - C{\cdot}10\,\text{mL}}\right]{\cdot}100 \quad (1)$$

where:

*m*PRO – PRO hydroxide amount used to prepare PRO solution for PRO loading procedure, 100 mg,

*m*MOF – MOF mass used for preparation of PRO@MOF composite, 100 mg,

C – Propranolol concentration in the filtrate (mg/mL).

2.3. Propranolol release profiles

The release of PRO from PRO@MOF composites was carried out based on the following procedure: 10 mg of PRO@MOF composite was placed in a plastic cup, then 40 mL of liquid medium (demineralised water or Simulated Body Fluid) was added. The PRO release was performed on a magnetic stirrer, maintaining human body temperature (36.6 °C). Samples of 0.5 mL of the medium solution were taken after a certain period, and subsequently subjected to UV–Vis analysis and replaced with fresh liquid medium. For UiO-67, due to the structure collapse in the SBF medium, the PRO release was measured by using the Thermo Vanquish Core HPLC System equipped with DAD and FL detectors and Accucore C18 150 × 3.0 mm^2 2.6 μm column. A mobile phase consisting of a solvent mixture of 0.25 mM solution of ammonium formate in 0.1 % formic acid (solvent A) and acetonitrile (solvent B) was used. Gradient elution was performed at a constant 0.6 mL/min flow rate as follows: from 0 min to 4.87 min, solvent A was used at 95 to 45 %, then from 4.87 min to 5.29 min the amount of solvent A began to increase from 45 to 95 %. The total measurement time was 10 min. During this time, the column was thermostated at 30 °C. The peak response of propranolol was recorded at 290 nm using a UV detector.

2.4. In vivo studies

2.4.1. Zebrafish maintenance

Danio rerio of the AB strain (Experimental Medicine Centre, Medical University of Lublin, Poland) were maintained according to the procedure described in the work of Kozioł *et al.* [41]. For the experiments, the embryos were treated with PRO (1–100 mM), 4-MMC (200 μM) alone and with PRO, (10 mM), MOFs or PRO@MOFs in a sterile zebrafish medium (E3) at 28.5 °C, for 96 h. Stock solutions of drugs were prepared in the E3 (pH = 7.1–7.3; 5.0 mM NaCl, 0.17 mM KCl, 0.33 mM $CaCl_2$, 0.33 mM $MgSO_4$) and diluted to the final test concentrations immediately before the experiments. Immediately after the experiment, larvae were killed by immersion in 15 μM tricaine methanesulfonate solution. All experiments were conducted in accordance with the National Institute of Health Guidelines for the Care and Use of Laboratory Animals and the European Community Council Directive for the Care and Use of Laboratory Animals of 22 September 2010 (2010/63/EU). For the experiment with larvae up to 120 hpf, the agreement of the Local Ethical Commission is not required. The concentrations of compounds were chosen based on our preliminary studies (Supporting Information file).

2.4.2. Cardiotoxicity

To determine the influence of PRO@MOFs on cardiac effects induced by 4-MMC, newly fertilised zebrafish eggs were exposed to compounds for a period of 96 h. The system applied in the experiment was static, as the changes in solution concentrations did not exceed the range of 20 % of nominal concentration values.

The experiment was performed in 24-well plates, with five embryos per well, and 10 per group. Each experiment was triplicate. Each plate was covered and kept in an incubator set at 28 ± 0.5 °C. Every 24 h, acute toxicity was determined based on a positive outcome of lethality. Death was judged by the coagulation of embryos or the absence of a heartbeat. At 96 hpf, heart rate was measured. The larvae were equilibrated at room temperature for 30 min and the heartbeats were counted under a stereomicroscope for 20 s. Obtained values were multiplied by three to obtain the number of beats per minute (bpm).

2.4.3. Locomotor activity

Evaluation of locomotor activity assay was performed in 96 hpf larvae. Larvae were incubated in 200 μL of E3 solution, each compound, or their combinations for 96 h. 30 min before the test larvae were transferred into 96 multi-well plates, one larva in each well (Supporting Movie). EthoVision XT v ideo tracking software (Noldus) was used for the evaluation of the locomotor activity of zebrafish larvae. The distance moved in a 10 min period was calculated in a light condition.

Immediately after the experiment, larvae were euthanised by immersion in the 15 μM of tricaine methanesulfonate (Sigma Aldrich) solution.

Data were analysed using one-way and two-way analysis of variance (ANOVA) followed by Tukey's post-hoc test or Bonferroni's post-hoc test, respectively. The confidence limit of $p < 0.05$ was considered statistically significant. The analysis was carried out using Prism v8.3.1 from GraphPad software.

3. Results and discussion

3.1. Materials synthesis and characterisation

For this study, four types of MOF materials were selected and then synthesised: UiO-66, UiO-67, MOF-808, and NU-1000. Common features of the selected materials were Zr_6-oxo-clusters bridged by polyethylene linkers [42]. The presence of different types of ligands in MOFs determines their different topologies, number, and pore sizes. The following organic acids served as ligands: benzene-1,4-dicarboxylic acid (H_2BDC) for UiO-66 [32], 1,1′-biphenyl-4,4′-dicarboxylic acid (BPDC)

for UiO-67 [38], 1,3,5-benzenetricarboxylic acid (H_3BTC) for MOF-808 [39], and tetraethyl 4,4′,4″,4‴-(pyrene-1,3,6,8-tetrayl)tetrabenzoic acid (H_4TBAPy) for NU-1000 [40]. Evaluation of the validity of the syntheses, and thus the crystallinity of the MOFs, was carried out using powder X-ray diffractometry (PXRD). The experimental results of pristine MOF (Figure S1A) were compared with literature data [32,40,43–45] and the high crystallinity of the parent MOFs was confirmed. Additionally, the PXRD analysis was carried out on PRO@MOF composite materials (Fig. 2A). All composites except PRO@UiO-67 showed structural stability and retained their crystalline character. The loss of crystallinity of the PRO@UiO-67 composite is due to the presence of an extended linker that builds the MOF structure. The extended biphenyl carboxylate linkers in MOF structure favour the clustering of water molecules close to the Zr nodes, resulting in the rotation of extended linkers and structure collapse [46]. However, low stability does not necessarily eliminate the potential use of the UiO-67 in PRO-controlled delivery. The gradual degradation of PRO@UiO-67 composite may be advantageous in the case of co-administration of combined drugs, during which adsorption of one of them in the MOF structure would be possible.

The porous properties of prepared MOFs were determined by low-temperature N_2 adsorption. Based on the equilibrium points of nitrogen adsorption, adsorption isotherms were plotted (Fig. 2B). Structural parameters determined by low-temperature N_2 adsorption are provided in Table 1. The specific surface areas of S_{BET} and S_L were determined based on the multi-layer and single-layer filling models, respectively [47,48]. In NU-1000 and UiO-67 the S_{BET} value was equal to approx. 2000 m^2/g. The total volume of micropores (NLDFT) was between 0.9 cm^3/g and 1.3 cm^3/g. Lower values of structural parameters were obtained in UiO-66 and MOF-808 materials. The specific surface area of S_{BET} was 1380 m^2/g and 1200 m^2/g, respectively. The volumes of micropores, on the other hand, were about 0.6 cm^3/g. Fig. 2C shows the pore volume distribution (NLDFT), from which it can be observed that all materials had pores with diameters in the range between 1.0 nm and 2.0 nm. The NU-1000 had developed additional pores in the range of 3.0–4.0 nm. The specific surface area of PRO@MOF composites drops significantly when compared with their pristine counterparts. The decrease of surface area and pore volumes in all prepared composites confirms successful PRO loading in PRO@MOF composite samples. The most significant change was observed for the PRO@UiO-67 sample, where S_{BET} decreased from 1962.8 m^2/g to 12.1 m^2/g, which may indicate either structure collapse or complete pore blockage by PRO molecules. On the other hand, for the PRO@NU-1000 sample, the decrease in S_{BET} is not as spectacular as for the PRO@UiO-67 sample despite comparable PRO loading (*cf.* Table 1). This phenomenon is related to large NU-1000 pore sizes and pore volumes that facilitate high PRO loading.

To determine the PRO encapsulation in prepared PRO@MOF samples, comparative thermogravimetric analysis was performed (Figure S3). All tests were carried out under analogous measurement conditions and with the same weight as the tested samples. The analysis

Table 1
Sample characterisation details.

	PRO loading wt.%	S_{BET} m^2/g	S_L m^2/g	V_{DFT} cm^3/g	D_{BJH} nm
UiO-66, (PRO@UiO-66)	7.4	1377.2 (393.7)	1868.3 (506.6)	0.632 (0.161)	2.9 (2.4)
UiO-67, (PRO@UiO-67)	58.0	1962.8 (12.1)	2586.2 (30.1)	0.891 (0.010)	3.3 (1.1)
MOF-808, (PRO@MOF-808)	7.5	1197.7 (388.6)	1696.0 (497.3)	0.611 (0.180)	3.1 (2.0)
NU-1000, (PRO@NU-1000)	52.5	2005.3 (1869.1)	4269.1 (3356.1)	1.289 (1.132)	3.7 (3.5)

of TGA curves for the PRO sample shows two characteristic mass losses in two temperature ranges, *i.e.*, from room temperature to 350 °C (about −85 % of the sample mass loss) and from 350 °C to 650 °C (about −15 % of the tested sample mass loss). Describing the recorded effects regarding a two-stage combustion process of the tested substance, PRO seems appropriate. By analysing the DSC curve, it is also concluded that an effect related to the melting process of the test drug takes place [49]. Subsequently, at higher temperatures, the curve indicates the presence of two exothermic effects, the nature of which, combined with the TGA result, clearly indicates a two-stage oxidation process taking place. For all measured samples, two main stages of mass change were found on the TG curves. Each time up to 100 °C, the weight loss is related to the removal of the adsorbed water (dehydration process). A further two-stage mass loss of the tested materials occurs at higher temperatures. The temperature ranges are similar, while the amount of weight loss of the samples differs for the different substances. It is claimed that the registered processes are related to the degradation of the linker and, finally, the degradation of the structure of the tested substances to ZrO_2.

The first mass loss stage (Figure S3) was the largest for the MOF-808 sample (about −37 %), and the smallest for the UiO-67 sample (about −11 %). The second stage of mass change was the most intense for NU-1000 (about −52 %) and UiO-67 (about 51 %), while the slightest change in mass was shown by samples MOF-808 (about −24 %) and UiO-66 (about −31 %).

In each case described above, the samples after the encapsulation process showed a more significant mass change when compared with the pristine samples. In temperatures up to 350 °C, the following weight changes of the tested samples were recorded before and after the encapsulation process - PRO@UiO-66: ca. –22 % to −24 %, PRO@MOF-808: ca. −37 % to −62 %, PR@NU-1000: ca. –23 % to −68 %, and UiO-67: ca. −11 % to −14 % weight loss, respectively.

The quantitative loading of PRO into the MOF structure was measured experimentally by UV–Vis spectroscopy. For PRO@NU-1000 and PRO@UiO-67, the amount of loaded PRO was equal to 52.5 and

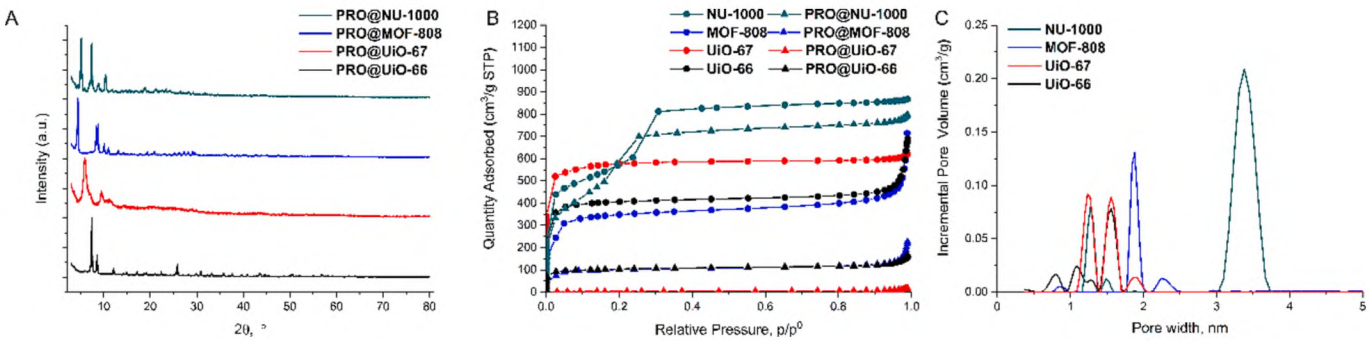

Fig. 2. Characterisation results of prepared samples (**A**) PXRD; (**B**) N_2 adsorption isotherms; (**C**) NLDFT pore size distribution.

58.0 wt%, respectively. The lower PRO loadings were achieved for PRO@UiO-66 and PRO@MOF-808 and oscillated around approx. 7 wt% in both composite samples. A dependence of the increase in drug loading with increasing pore volume of Zr-MOFs was observed. The relationships described, along with the results, are shown in Table 1.

The molecular nature of pristine and composite PRO@MOFs samples was determined by FTIR spectroscopy (Fig. 3). The spectrum of PRO reveals a broad and characteristic band in the range of 1350 cm^{-1} to 1260 cm^{-1} originating from asymmetric stretching vibrations of =C-O-C- alkyl aryl ether present in the structure of PRO [50,51]. The band at 3282 cm^{-1} may be attributed to NH stretching vibrations from the amine group. In addition, the band present on the spectrum near 2947 cm^{-1} is characteristic of the alkane group and supports the identification of PRO [50]. The band at 1103 cm^{-1} corresponds with the stretching vibrations of the aryl alkyl ether. The peak at 771 cm^{-1} is typical of α-substituted naphthalenes [51]. Other peaks characterising PRO are the peak at 1579 cm^{-1}, originating from the aromatic C=C bond, and the peak from the aromatic C-H bond at about 3049 cm^{-1} [50]. The spectra of pristine MOFs, specifically UiO-66, UiO-67, MOF-808, and NU-1000, are typical spectra for Zr-MOFs and are in good agreement with those in the literature [38,45]. The typical broad band in the 3600–2600 cm^{-1} region is attributed to OH vibrations from adsorbed water [50,51]. The carboxyl group, and more specifically, the in-phase and out-of-phase stretching vibrations, were confirmed by the bands at 1585 cm^{-1} and 1390 cm^{-1}. In the 1750–1000 cm^{-1} range, the bands of carboxyl and heterocyclic C=C stretching vibrations were observed [38,52]. Additionally, the band at 3000 cm^{-1} is identified with C-H bond vibrations in the benzene ring [38]. For UiO-67, an additional band at 3675 cm^{-1} was observed, originating from vibrations of the isolated OH group [38]. Bands in the range of 750–650 cm^{-1} correspond to bending vibrations of C-H and O-H and Zr-O [38]. The FTIR spectra of PRO@MOFs composites show bands characteristic for both pristine MOFs and introduced PRO, which on the one hand confirms that the introduction of the drug into the structure was successful, and on the other hand that the MOFs remained stable. It was observed that particularly characteristic bands at 1269 cm^{-1} and 1236 cm^{-1} were present on the spectra and correspond with the asymmetric stretching vibrations of =C-O-C- alkyl aryl ether [50–52]. In Fig. 3, the characteristic regions for PRO vibrations are labelled as PRO markers. The intensity of the two bands on the spectrum is dependent on the amount of PRO that was introduced to the MOF structure, and increases simultaneously as the degree of PRO loading into the MOFs structure increases. The intensity of the bands increases sequentially for PRO@UiO-66, PRO@MOF-808, PRO@UiO-67, and PRO@NU-1000. For the PRO@UiO-66 (Fig. 3A) and PRO@MOF-808 (Fig. 3C) composites, the bands at 1269 cm^{-1} and 1236 cm^{-1} are faintly visible, which is related to the low amount of PRO in the PRO@MOFs composites. In the case of the other two samples, PRO@UiO-67 (Fig. 3B) and PRO@NU-1000 (Fig. 3D), the PRO bands are characterised by significant intensities, which corresponds to the higher amount of PRO loaded into the MOF structure.

The μRaman characterisation results are shown in Fig. 4. The bands characteristic for PRO were detected at 1380 cm^{-1} and 733 cm^{-1} and are attributed to the naphthalene ring vibrations. The former corresponds with νC-C vibrations. According to the literature, the

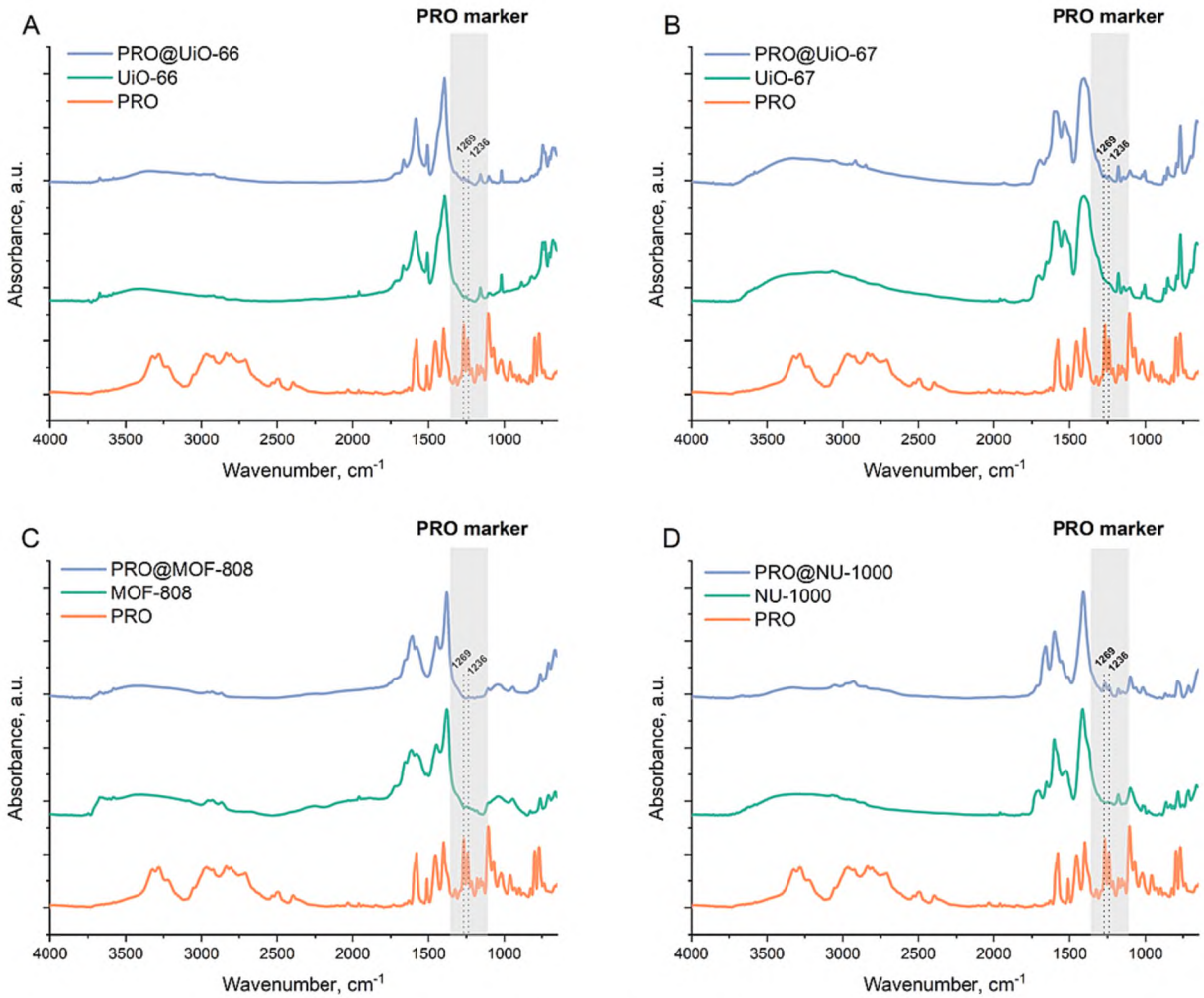

Fig. 3. Transmission FTIR spectra of prepared samples; **(A)** PRO@UiO-66; **(B)** PRO@UiO-67; **(C)** PRO@MOF-808; **(D)** PRO@NU-1000.

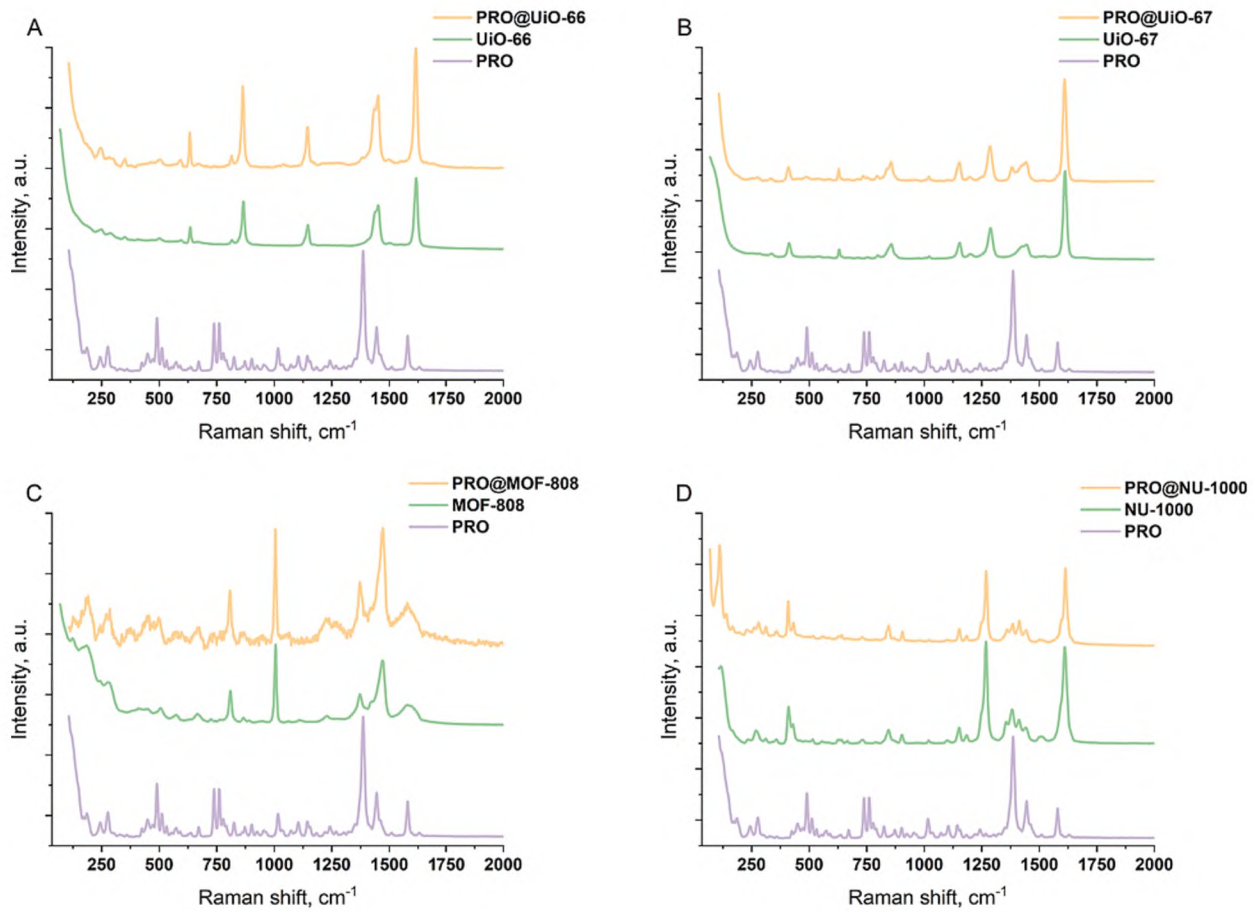

Fig. 4. μRaman spectra of prepared samples.

characteristic bands at 1560 cm^{-1} and 1423 cm^{-1} originate from νC-C and C-H vibrations [53]. In the case of UiO-66, bands at 1615 cm^{-1}, 1447 cm^{-1}, and 1142 cm^{-1} are visible, corresponding to C=C stretching vibrations, terephthalate ring breathing, and ring deformation [54]. Pristine UiO-67 exhibits bands at 1609 cm^{-1}, 1447 cm^{-1}, 1286 cm^{-1}, 1151 cm^{-1}, 855 cm^{-1}, and 631 cm^{-1}. The band at 1286 cm^{-1} originates from C-C ligand interring stretching. The band at 855 cm^{-1} is associated with symmetric C-C breathing, while 631 cm^{-1} originates from the in-plane bending of the C-C aromatic ring [55]. Considering MOF-808, the bands at 807 cm^{-1} and 570 cm^{-1} correspond successively to O-H bond vibrations and/or symmetric C-C breathing and C-C-C in-plane bending [56]. The NU-1000 exhibits bands at 1180 cm^{-1}, 1150 cm^{-1}, and 900 cm^{-1} which may be attributed to pyrene-based ligand vibrations [57]. The μRaman spectra of PRO@MOF composite materials allowed us to confirm the presence of PRO in prepared composites. The characteristic bands for PRO in MOF materials are 1380 cm^{-1} and 733 cm^{-1} attributed to the C-C vibrations of the naphthalene ring. These bands are most prominent for PRO@UiO-67, PRO@UiO-66, and PRO@MOF-808, all being characterised by much lower intensity. For the PRO@NU-1000 sample, they are practically invisible. This is related to the large number of other peaks originating from the extended MOF ligand.

The application of scanning electron microscopy (SEM) allowed us to evaluate the morphology of PRO@MOFs composites (Fig. 5). For pristine MOFs, surface morphology data are widely available and very well described in the literature [32,52,58]. For example, the use of UiO-66 with hydrochloric acid as a modulator is associated with a higher number of structural defects and a change in crystal size, compared to classical "defect-free" UiO-66 [32,52]. This confirms the literature data on the effect of modulator concentration and acidity on MOF morphologies [52]. In addition, PRO@MOF-808 exhibits nanocrystal sizes in the 150–350 nm range, as seen when comparing Figure S4C and Fig. 5C [58]. Additionally, UiO-67 exhibits agglomerated crystals in a *ca.* 1 μm size with visible crystal cracks. The SEM images confirm that NU-1000 is characterised by the largest crystal size. The prepared PRO@NU-1000 are detected as rod-shaped microcrystals or hexagonal prisms with 3 μm diameter.

3.2. Prolonged propranolol release in different media

PRO release profiles from PRO@MOFs composites were determined in two types of media: demineralised water and Simulated Body Fluid (SBF). The results are shown in Fig. 6 (percentage release) and Figure S5 (PRO released in mg). When analysing the release of the drug into the distilled water medium at 36.6 °C, the highest amount of PRO release was observed for the PRO@UiO-66 and PRO@MOF-808 composites. The maximum amounts of PRO released reach 97 % and 41 %, respectively, after 24 h. Above that, the smallest amount of PRO was released from PRO@NU-1000, being equal to 23 %. The PRO@UiO-67 composites were characterised by a drug release of approx. 27 %. An atypical but at the same time intriguing correlation is that PRO@UiO-66, when loaded with PRO, is characterised by the lowest amount of drug and the highest release, in contrast to PRO@NU-1000, where loading is high, and release is low. This dependency is shown in Fig. 6A. In each case, the release of PRO into distilled water occurs rapidly. After less than 30 min, most of the drug has already been released from each composite, and after 24 h a plateau is reached. The results of PRO release to the SBF solution are shown in Fig. 6B. Regarding the percentage amount of released PRO, the highest values are observed for PRO@UiO-66 and PRO@UiO-67 (95 % and 90 %, respectively). Significantly smaller

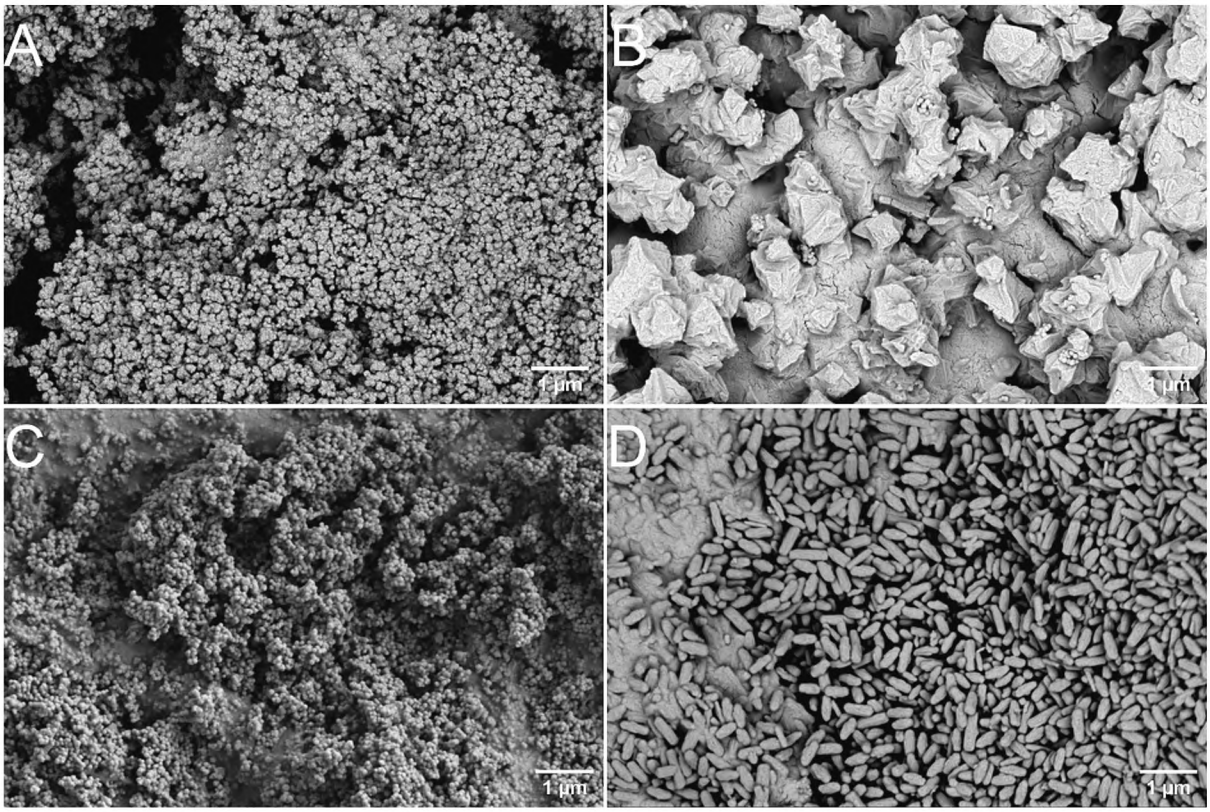

Fig. 5. SEM images of prepared samples; **(A)** PRO@UiO-66, **(B)** PRO@UiO-67, **(C)** PRO@MOF-808, **(D)** PRO@NU-1000.

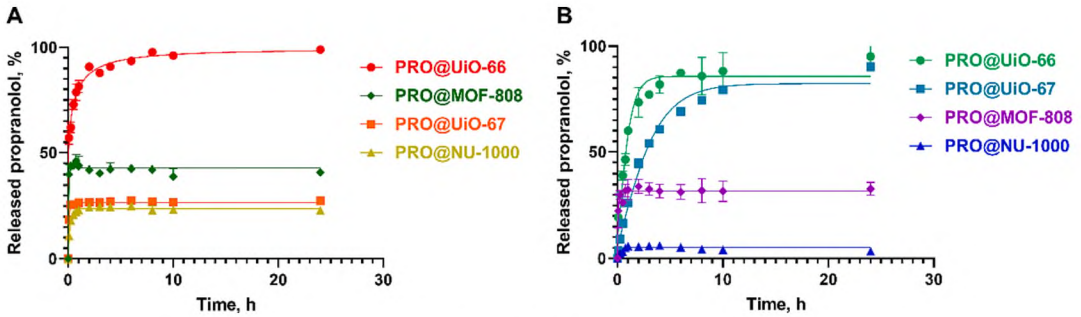

Fig. 6. PRO release profiles in different media; **(A)** H_2O; **(B)** SBF.

amounts of released PRO are shown by PRO@MOF-808 and PRO@NU-1000, with values of about 30 % and about 5 %, respectively. For all composites except PRO@UiO-67, we observe a reduction in the amount of released PRO in the SBF medium compared to distilled water. The highest inhibition of PRO release occurs for PRO@NU-1000, as the value of released PRO drops from 23 % in distilled water to 5 % in SBF. A similar relation was observed by us in our previous studies [32]. Above that, H. Dong *et al.* [59], also observed a decrease in the amount of released drug in a PBS environment of pH = 7.4. It has been confirmed that the ionic environment influences a decrease in the stability of the MOF structure, especially under more alkaline conditions [60,61]. When focusing on drug release, it is important to consider not only the higher instability at higher pH, but especially the effect of the ionic environment on drug-framework interactions of MOFs. The presence of ions in the medium can promote ion exchange between the drug and the anions in the solution, which can in turn be a limiting factor in the release of the drug from the structure. Ions dissolved in the SBF (Cl^-, SO_4^{2-}, HCO_3^-, HPO_4^{2-}) may impede the exit of the drug from the MOF structure, thus being the reason why less drug is released into the medium [61]. A completely different situation is observed in the case of drug release from PRO@UiO-67. The amount of released PRO from PRO@UiO-67 is higher when SBF is used. This phenomenon may be caused by the gradual MOF structure collapse in the SBF solution by the mechanisms described in the work [46]. However, the gradual PRO@UiO-67 structure degradation may be beneficial in terms of the prospective application of PRO@MOF composites in living organisms. The gradual MOF structure degradation followed by the PRO release may favour easier removal of MOFs from living organisms when considering their potential oral administration. Despite the 15–300 nm size of prepared PRO@UiO-67 composite their further degradation may even reduce the crystal size, which will allow MOF residue removal by, *e.g.*, kidney filtration. Additionally, when considering the potential application of PRO@MOF composites in an acute overdose or controlled withdrawal, several drugs may be administered, thus competitive drug adsorption may not be favourable.

Considering the potential application of selected Zr-MOFs as efficient PRO carriers for 4-MMC detoxification or supervised withdrawal, the toxicity of linker and node species should be taken into account. In the

case of the MOF showing relatively low chemical stability, the degradation products, i.e., the inorganic and organic building blocks, may slowly diffuse intercellularly and cause a local increase in concentration of metals and organic linkers [62]. Over the years, numerous MOFs have been examined for their toxicity using various cell lines and animals. For the top 10 MOF, including MOF-5(Zn), HKUST-1(Cu), UiO-66(Zr), MIL-100(Fe), ZIF-8(Zn), MIL-88A(Fe), MIL-88B(Fe, Cr), MIL-101(Fe, Cr), MOF-74(Co, Ni, Mg, Cu, Mn, Zn) and UiO-67, however, the literature information on cytotoxicity is scarce [63] In the recent work of Yang *et al.* [64], the acute toxicity and biodistribution of ZrO_2 were tested *in vivo* by intravenous injection. The authors revealed that a higher concentration of zirconium was detected in the liver than in the spleen or other organs and that the zirconium concentration in the range of 10–350 mg/kg may be considered safe. In the work by Ruyra *et al.* [63] the toxicity of 16 selected representative nano-MOFs, including nano-UiO-67 and nano-UiO-66, was tested *in vivo* and *in vitro* using human hepatocyte (HepG2) and breast cancer (MCF7) cell lines, and the zebrafish model. To determine the concentration of zirconium ions that may migrate from MOF structure to the surroundings, selected nano-MOFs were dispersed in 10 mL of DMEM with 10 % fetal bovine serum and the concentration of solubilised metal ions was measured by ICP-OES spectroscopy. The authors developed a five-grade toxicity scale (0: no toxicity, 4: maximum toxicity) to qualitatively compare selected nano-MOFs. The authors found that Co^{2+}, Ni^{2+}, Zn^{2+}, Zr^{2+}, or Mg^{2+} salts did not show any significant cytotoxicity in the *in vitro* tests using two HepG2 and MCF7 human cell lines. Similarly, in the *in vivo* experiments using zebrafish embryos, both nano-UiO-66 and nano-UiO-67 revealed hardly any cytotoxic effects.

For the organic linker toxicity, the "rule of thumb" was introduced in the work by Ettlinger *et al.* [62], where the toxicity increases from fumaric acid (considered the most biocompatible) through trimesic acid, terephthalic acid, and nitro- and tetramethyl-terephthalic acids. It must be emphasised, however, that the toxicity of the individual MOF organic linker should be determined individually, depending on the MOF used. In recent works, the toxicity of the most utilised organic linkers such as terephthalic acid, 1,1′-biphenyl-4,4′-dicarboxylic acid (organic linkers for UiO-66, UiO-67, respectively), and 1,3,5-benzenetricarboxylic acid (MOF-808) was tested using the various cell lines including mammal J774A.1 cells, carcinoma cell line HT-29, and the human breast carcinoma cell line MCF-7 [62], A549, and (B) MH-S cell lines [65], showing no significant toxicity of organic linkers building MOF structure.

Propranolol adsorption – a molecular approach

The DFT calculations were performed with the use of the VASP [66] code to determine the adsorption sites of guest molecules in the frameworks of the studies MOFs. The computational methodology is described in detail in the Supporting Information file, while the representative and optimised structure of NU-1000 with adsorbed PRO molecules is shown in Fig. 7. The π-π orbital stacking was used as a geometrical descriptor of the molecule-framework interactions (see Fig. S6) and it was determined by the analysis of the least square fit of the planes of the aromatic rings thereof. The angles and distances between the aromatic rings of PRO and MOF linkers were found typical for the systems with pronounced π-π stacking. The interaction of the electronic structures of the aromatic rings of the PRO molecule and the MOF linker was also studied in the view of the charge transfer between the interacting systems, and the covalent bond order between them (see Table S6).

The sorption loading of PRO in the MOF structures, studied by forcefield-based, rigid host MC, was found to be the highest (25 molecules per 1 unit cell of MOF) for NU-1000 and only 4 for UiO-67 (see Table S3). In the case of the "defect free" UiO-66, no PRO sorption was possible. To resolve the discrepancy between the MC modelling and the experiment, three defective structures of UiO-66 were studied: one with the Zr cluster missing, one with the linker removed and one with the Zr cluster and the adjacent linker missing (see Table S3). Sorption was found to be possible only for the latter two structures. Even though the small amount of PRO was found to be able to adsorb in the latter case, the sorption was weak, with $E_{ads} = -0.409$ eV, and no π-π stacking is observed. Much stronger adsorption was found for the other studied MOFs, namely for MOF-808, UiO-67, and NU-1000, E_{ads} was −0.920 eV, −1.106 eV, and −1.183 eV, respectively.

To assess the relationship between the material properties and the adsorption performance, RDA analysis was carried out for the following inputs: pore size (RDA 1) and S_{BET} (RDA 2) for the composites, and the

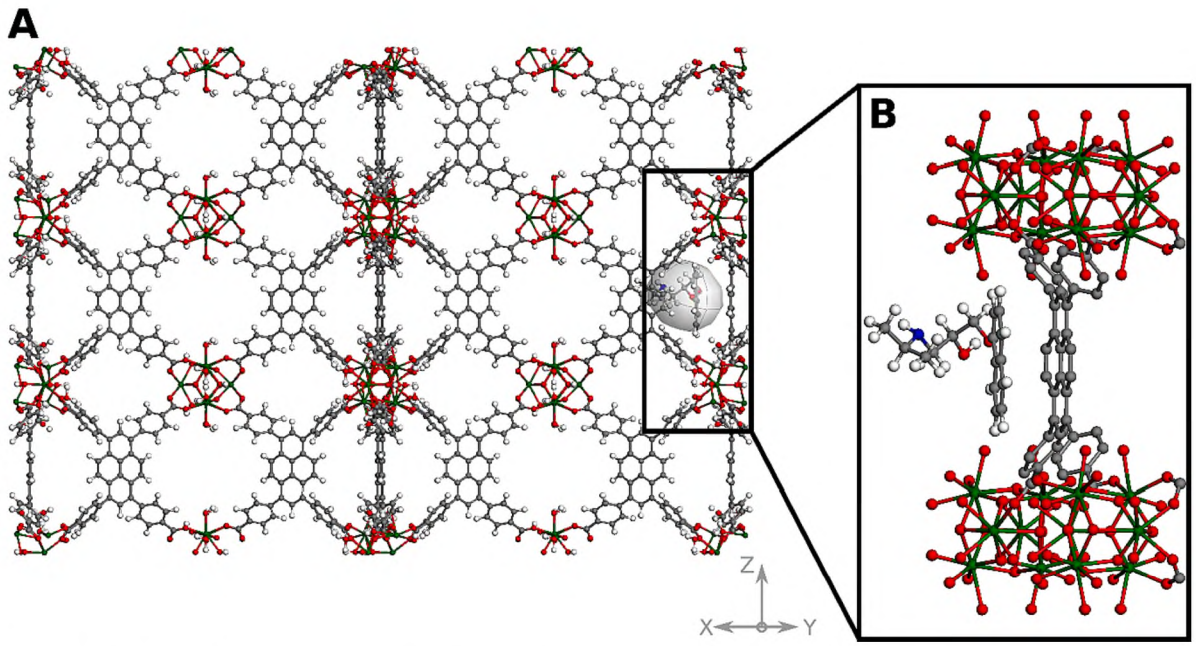

Fig. 7. DFT optimised structure of NU-1000, with four Zr_6 nodes bonded to the linker (zoomed area), with adsorbed PRO molecule (ellipsoid); **(A)** general model, **(B)** zoomed large channel with adsorbed PRO; hydrogens in MOF framework omitted for clarity; green – Zr, red – O, grey – C, blue – N; additional DFT optimised structures are provided in the Supplementary Information file. (For interpretation of the references to colour in this figure legend, the reader is referred to the web version of this article.)

following outputs: maximum PRO release (at 24 h) and PRO loading (see Figure S7). By analysis of the RDA graph, the direct relationship between the structural parameters and the PRO loading and maximum PRO release cannot be found, and the PRO release is controlled by the molecular forces as revealed above from DFT analyses. However, due to the low number of points, such analysis is statistically of limited significance.

The 100 ns molecular dynamic (MD) simulation was performed using the Gromacs 2019.4 program [67,68]. The DFT-optimised structure of the PRO@MOF complex was used as the initial configuration (Fig. 8). The computational methodology is described in detail in the Supporting Information file. The MD study shows that the 3D structures of MOF crystals were slightly deformed due to interactions with the drug (Fig. 8). The reason may also be the presence of water in the studied system. However, throughout the simulation time (100 ns), PRO molecules remain inside the pores and adopt conformations different from that DFT-optimised, and π-π interaction is no longer observed at all or in an altered T-shape geometry (Fig. 8, S8 and Supporting Movies). In the case of MOF-808 (Fig. 8E and F), due to the largest channel size, PRO molecules can move most freely. During the simulation, the drug was able to diffuse only along the pores, in the direction along the Z axis in Fig. 8 and S8. The plots of the Mean Square Displacement (MSD(t)) dependence (Figure S9) show that the propranolol molecules moved very slightly, and the movement was noticeable only in the case of MOF-808. The calculated diffusion coefficients (D_A) (Figure S9) increase from UiO-67, NU-1000, and MOF-808 series, and are equal to $0.00026 \cdot 10^{-5}$, $0.00039 \cdot 10^{-5}$, and $0.00047 \cdot 10^{-5}$ cm^2/s, respectively, which further confirms the above observations. In summary, the drug's movements are only due to the change in its conformation within a single pore (cf. Fig. 8). This means that this moderately lipophilic compound (logP = 3.10) could not diffuse so extensively and freely in the porous material in an inert aqueous environment.

It should be emphasised here that the computationally obtained maximum sorption capacity is dependent not only on the binding energy and the volume of the cages in the sorbent framework, but also on the shape of the cages. The experimental sorption capacity depends also on the cage availability to the sorbate molecules, i.e., the dimension of the channels, which is reflected in Table S5.

3.3. *Controlled PRO delivery from MOF composite reduces mortality and locomotor activity - in vitro and in vivo experiments*

The complementary characterisation of prepared samples to be used as a novel detoxification material in 4-MMC overdose or controlled withdrawal involved *in vivo* studies of pristine MOFs, PRO, PRO@MOFs composites, and 4-MMC (Fig. 9, Figure S10-S11).

The MOFs used in this study including MOF-808, UiO-66, UiO-67, and NU-1000 showed mortality of 3.57 %, 24.14 %, 35.48 %, and 25.81 %, respectively (Fig. 9A). 4-MMC (200 μM) combined with PRO (10 mM) exerted mortality at the level of 17.39 %. Combined treatment using 4-MMC with PRO@MOFs resulted in mortality at the following levels: 4-MMC + PRO@MOF-808 – 3.33 %; 4-MMC + PRO@UiO-66–28.57 %; 4-MMC + PRO@UiO-67–10 % and 4-MMC + PRO@NU-1000–6.67 % (Fig. 9A). All living larvae hatched correctly (data not shown).

Materials displayed changes in heart rhythm (Fig. 9B). Two-way ANOVA showed statistically significant changes in the interaction F (9, 564) = 5.599, P < 0.0001; PRO@MOFs treatment F (9, 564) = 17.97, P < 0.0001 without 4-MMC effect F (1, 564) = 2.494, P = 0.1163). A post-hoc Bonferroni test showed that PRO ($p < 0.01$) decreased, and 4-MMC ($p < 0.01$) increased the heart rate when compared to E3 treated groups. Furthermore, PRO@MOF-808 increased heart rate in comparison with the PRO-treated group ($p < 0.01$). 4-MMC + UiO-67 ($p < 0.01$), 4-MMC + NU-1000 ($p < 0.001$), 4-MMC + MOF-808 ($p < 0.001$), 4-MMC + PRO ($p < 0.0001$), 4-MMC + PRO@MOF-808 ($p < 0.001$), 4-MMC + PRO@UiO-66 ($p < 0.0001$), 4-MMC + PRO@UiO-67 ($p < 0.0001$) 4-MMC + PRO@NU-1000 ($p < 0.0001$) decreased heart rate in comparison with the 4-MMC treated group, 4-MMC + PRO@MOF-808 ($p < 0.05$) increased heart rate when compared to the 4-MMC + PRO group.

Two-way ANOVA showed statistically significant changes in locomotor activity (interaction F (9, 586) = 7.886, P < 0.0001, PRO@MOFs treatment F (9, 586) = 5.974, P < 0.0001 without 4-MMC effect F (1, 586) = 1.285, P = 0.2584). A post-hoc Bonferroni test showed that PRO ($p < 0.05$), and 4-MMC ($p < 0.0001$) increased distance travelled when compared to E3 treated groups, Combinations of 4-MMC with MOFs and PRO as well as PRO@MOFs decreased locomotor activity in comparison with 4-MMC treated group ($p < 0.0001$).

NPS potentially affects brain function and exerts cardiovascular side effects. Complementing laboratory rodents, the zebrafish (*Danio rerio*) is a powerful animal model organism for screening neuroactive and cardiotoxic drugs, e.g., amphetamines. Here, we tested a series of four PRO@MOFs and their ability to reverse cardiac, as well as the toxic effects of 4-MMC in the zebrafish larvae. Overall, PRO was shown to reverse the 4-MMC-induced increase in heart rate. However, we observed increased mortality of larvae subjected to the coadministration of the above-mentioned drugs. Our studies showed that incorporation of PRO into the MOF structure alleviates the cardiotoxic and neurotoxic effects of 4-MMC, observed as a decrease in heart rate and a decrease of distance swum by larvae, respectively. Interestingly, mortality was decreased when compared to PRO with 4-MMC-treated groups (without any MOFs). The exception was noticed for PRO@UiO-66 administered to 4-MMC intoxicated larvae, which was shown to be more toxic than 4-MMC with PRO itself.

4. Conclusions

Our study aimed to examine the possibility of using Zr-based MOF materials as an efficient PRO cargo for 4-MMC overdose and controlled withdrawal. PRO hydrochloride was efficiently loaded into selected Zr-MOFs and composites were formed: PRO@UiO-66, PRO@UiO-67, PRO@MOF-808, PRO@NU-1000. Due to the different porosity and crystallinity of the materials, the amount of PRO introduced into the MOFs varied significantly.

The kinetics of drug release from PRO@MOFs was studied, which allowed us to observe differences in the rate and amount of PRO released depending on the medium. We can conclude that the use of ion-rich solutions, such as SBF, has an inhibitory effect on the release of the PRO from the MOF structure. This is most likely due to increased ion exchange between the drug and the anions in the solution. On the other hand, the interaction of ions with the metal–organic framework affects the much slower and more gradual release of PRO, which may minimise the negative effects of its use. For drug release into water and SBF environments, PRO@UiO-66 was the most efficiently used, with more than 95 % of the drug released.

Based on the experimental and theoretical DFT and MD results, we can conclude that the Zr-based MOFs may be used successfully as an efficient PRO carrier. The use of PRO@MOF composites is an effective and safe solution, whereby the release of the drug occurs gradually, with high bioavailability and low cytotoxicity. Moreover, the side effects of PRO therapy are inhibited. Our studies, for the first time, presented the safety of PRO@MOFs in 4-MMC intoxication in a sensitive *in vivo* vertebrate model system, the zebrafish, raising the possibility of their potential use in NPS overdose and as a detoxification system for addicts.

Declaration of Competing Interest

The authors declare that they have no known competing financial interests or personal relationships that could have appeared to influence the work reported in this paper.

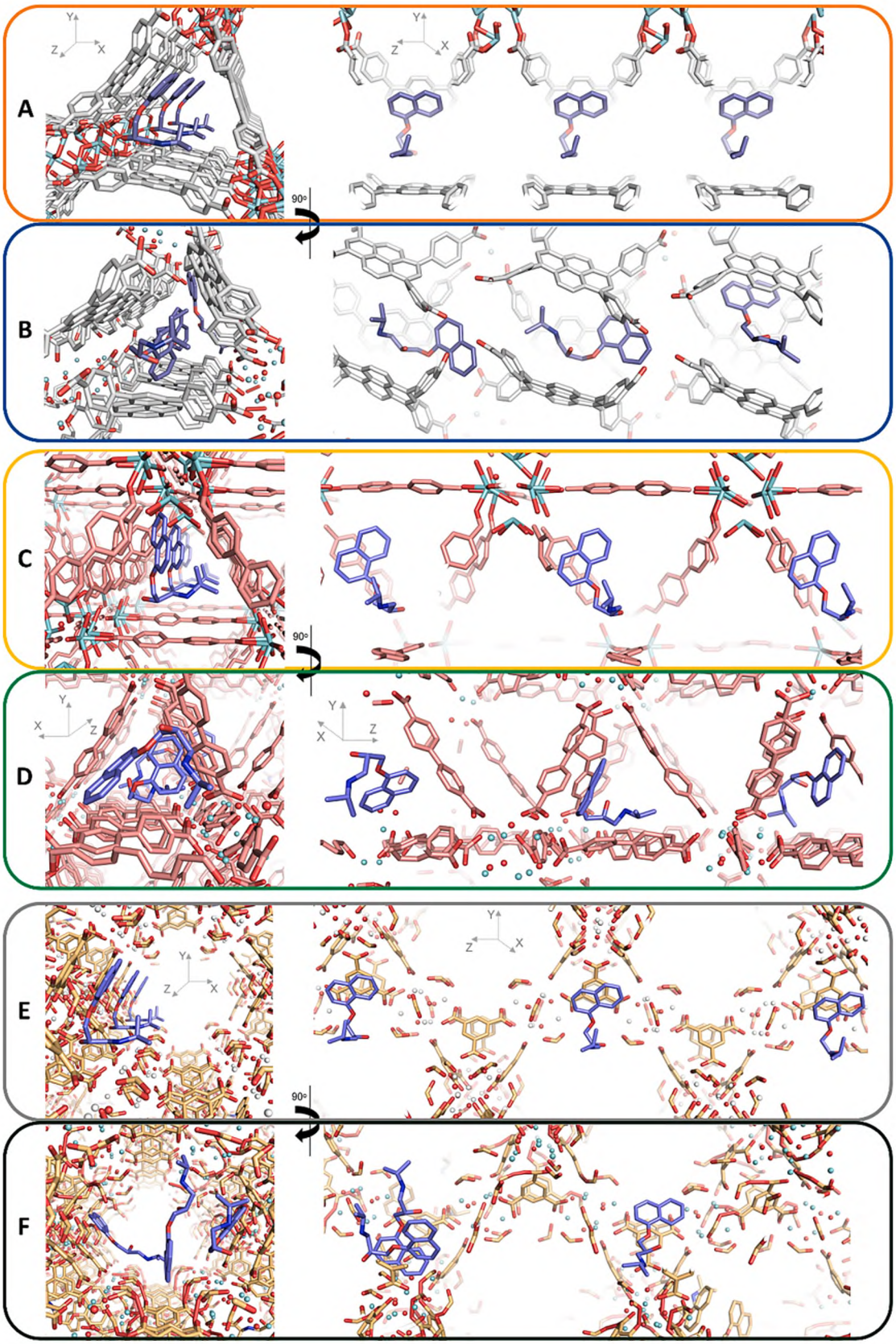

Fig. 8. Close-up views of the complexes of three propranolol molecules in the channel of MOFs. **(A, C, E)** Initial structure = DFT-optimised and **(B, D, E)** after 10 ns of the molecular dynamic simulation respectively for NU-1000, UiO-67, and MOF-808; green – Zr, red – O, blue – N, and grey, salmon, light orange or purple – C, respectively for MOFs and ligand molecules. Water molecules and hydrogen atoms are invisible. The corresponding super-cell views are provided in the Supporting Information File. (For interpretation of the references to colour in this figure legend, the reader is referred to the web version of this article.)

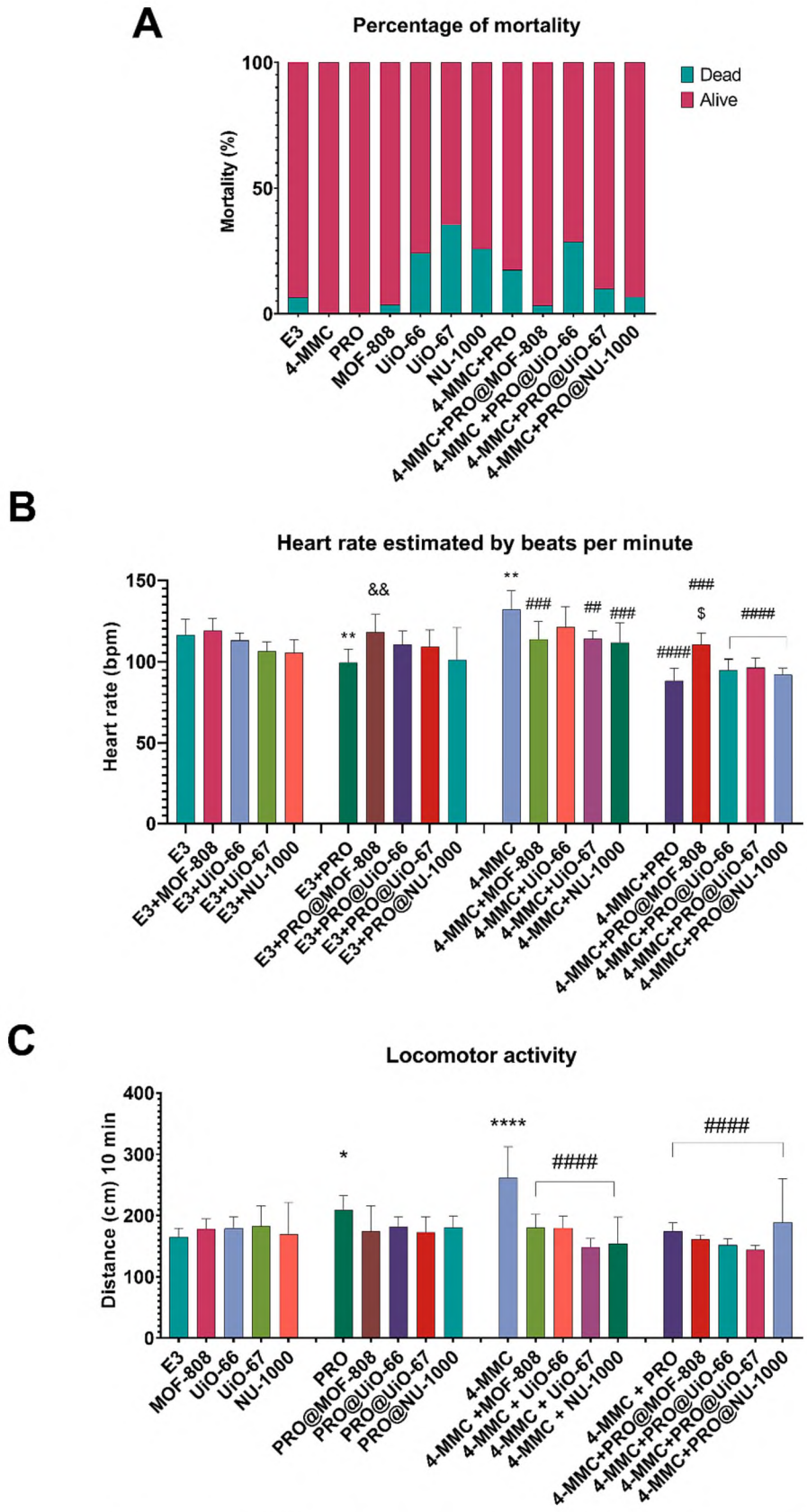

Fig. 9. Effects of 96 h exposure to compounds in zebrafish; (a) a percentage of mortality (b) heart rate estimated by beats per minute (c) locomotor activity; Data are presented as means ± SD; two-way ANOVA, n = 30; *p < 0.05, **p < 0.01, ****p < 0.0001 versus E3 control group; && p < 0.01 versus propranolol (PRO treated group ##p < 0.05, ###p < 0.001, ####p < 0.0001 versus 4-MMC (200 μM) group, $ p < 0.05 versus 4-MMC (200 μM) + PRO group, Bonferroni's test.

Data availability

Data will be made available on request.

Acknowledgement

The work was supported by the National Science Centre, Poland, under the research project "MOF-antidote: Novel detoxification materials based on metal-organic frameworks for drugs of abuse removal – synthesis, chemical characterisation, toxicity, and efficacy in in vivo and in vitro studies", no. UMO-2021/43/B/NZ7/00827. Thermal studies were performed within the framework of funding for statutory activities of AGH University of Krakow in Kraków, Faculty of Materials Science and Ceramics (16.16.160.557).

Appendix A. Supplementary data

Supplementary data to this article can be found online at https://doi.org/10.1016/j.cej.2023.147655.

References

[1] C.E. O'Rourke, B. Subedi, Occurrence and mass loading of synthetic opioids, synthetic cathinones, and synthetic cannabinoids in wastewater treatment plants in four U.S. communities, Enviromental, Sci. Technol. 54 (2020) 6661–6670, https://doi.org/10.1021/acs.est.0c00250.

[2] I. Mercurio, A. Pellegrino, L. Panata, F. Filippucci, P. Melai, A. Gili, D. Capano, G. Troiano, G. Rettagliata, M. Lancia, M. Bacci, Toxicological findings in fatal intoxications from synthetic cathinones: a narrative review, Aust. J. Forensic Sci. 54 (2022) 480–498, https://doi.org/10.1080/00450618.2020.1841291.

[3] M.C. Smid, T.D. Metz, A.J. Gordon, Stimulant use in pregnancy: an under-recognized epidemic among pregnant women, Clin. Obstet. Gynecol. 62 (2019) 168–184, https://doi.org/10.1097/GRF.0000000000000418.

[4] European Monitoring Centre for Drugs and Drug Addiction. European drug report 2017 - Trends and developments, Publications Office of the European Union, Luxembourg, 2017, https://doi.org/10.2810/610791.

[5] J. Mead, A. Parrott, Mephedrone and MDMA: a comparative review, Brain Res. 1735 (2020), 146740, https://doi.org/10.1016/j.brainres.2020.146740.

[6] A. Sakagami, T. Soeda, Y. Saito, K. Nakao, Y. Ozaki, K. Kimura, J. Ako, T. Noguchi, S. Suwa, K. Fujimoto, K. Dai, T. Morita, W. Shimizu, A. Hirohata, Y. Morita, T. Inoue, A. Okamura, T. Mano, M. Wake, K. Tanabe, Y. Shibata, M. Owa, K. Tsujita, H. Funayama, N. Kokubu, K. Kozuma, S. Uemura, T. Tobaru, K. Saku, S. Oshima, Y. Miyamoto, H. Ogawa, M. Ishihara, Clinical impact of beta-blockers at discharge on long-term clinical outcomes in patients with non-reduced ejection fraction after acute myocardial infarction, J. Cardiol. 81 (2023) 83–90, https://doi.org/10.1016/j.jjcc.2022.08.002.

[7] R.A. Caplan, J.P. Zuflacht, J.A. Barash, C.R. Fehnel, Neurotoxicology syndromes associated with drugs of abuse, Neurol. Clin. 38 (2020) 983–996, https://doi.org/10.1016/j.ncl.2020.08.005.

[8] C.W. Schindler, E.B. Thorndike, M. Suzuki, K.C. Rice, M.H. Baumann, Pharmacological mechanisms underlying the cardiovascular effects of the "bath salt" constituent 3,4-methylenedioxypyrovalerone (MDPV), Br. J. Pharmacol. 173 (2016) 3492–3501, https://doi.org/10.1111/bph.13640.

[9] Ł. Szeleszczuk, D. Frączkowski, Propranolol versus other selected drugs in the treatment of various types of anxiety or stress, with particular reference to stage fright and post-traumatic stress disorder, Int. J. Mol. Sci. 23 (2022) 10099, https://doi.org/10.3390/ijms231710099.

[10] R. Guo, X. Cai, H. Liu, Z. Yang, Y. Meng, F. Chen, Y. Li, B. Wang, In situ growth of metal–organic frameworks in three-dimensional aligned lumen arrays of wood for rapid and highly efficient organic pollutant removal, Environ. Sci. Technol. 53 (2019) 2705–2712, https://doi.org/10.1021/acs.est.8b06564.

[11] A. Hashemzadeh, F. Amerizadeh, F. Asgharzadeh, M. Darroudi, A. Avan, S. M. Hassanian, M. Landarani, M. Khazaei, Delivery of oxaliplatin to colorectal cancer cells by folate-targeted UiO-66-NH_2, Toxicol. Appl. Pharmacol. 423 (2021), 115573, https://doi.org/10.1016/j.taap.2021.115573.

[12] R. Cui, P. Zhao, Y. Yan, G. Bao, A. Damirin, Z. Liu, Outstanding drug-loading/release capacity of hollow Fe-metal-organic framework-based microcapsules: a potential multifunctional drug-delivery platform, Inorg. Chem. 60 (2021) 1664–1671, https://doi.org/10.1021/acs.inorgchem.0c03156.

[13] H. Molavi, H. Moghimi, R.A. Taheri, Zr-based MOFs with high drug loading for adsorption removal of anti-cancer drugs: a potential drug storage, Appl. Organomet. Chem. 34 (2020), e5549, https://doi.org/10.1002/aoc.5549.

[14] J.W.M. Osterrieth, D. Fairen-Jimenez, Metal–organic framework composites for theragnostics and drug delivery applications, Biotechnol. J. 16 (2021) 2000005, https://doi.org/10.1002/biot.202000005.

[15] G. Chedid, A. Yassin, Recent trends in covalent and metal organic frameworks for biomedical applications, Nanomaterials. 8 (2018) 916, https://doi.org/10.3390/nano8110916.

[16] Y. Sun, L. Zheng, Y. Yang, X. Qian, T. Fu, X. Li, Z. Yang, H. Yan, C. Cui, W. Tan, Metal–organic framework nanocarriers for drug delivery in biomedical applications, Nano-Micro Lett. 12 (2020) 1–29, https://doi.org/10.1007/s40820-020-00423-3.

[17] X. Liu, T. Liang, R. Zhang, Q. Ding, S. Wu, C. Li, Y. Lin, Y. Ye, Z. Zhong, M. Zhou, Iron-based metal-organic frameworks in drug delivery and biomedicine, ACS Appl. Mater. Interfaces. 13 (2021) 9643–9655, https://doi.org/10.1021/acsami.0c21486.

[18] S. He, L. Wu, X. Li, H. Sun, T. Xiong, J. Liu, C. Huang, H. Xu, H. Sun, W. Chen, R. Gref, J. Zhang, Metal-organic frameworks for advanced drug delivery, Acta Pharm. Sin. b. 11 (2021) 2362–2395, https://doi.org/10.1016/j.apsb.2021.03.019.

[19] T. Tataranni, C. Piccoli, Dichloroacetate (DCA) and cancer: an overview towards clinical applications, Oxid. Med. Cell. Longev. 2019 (2019), https://doi.org/10.1155/2019/8201079.

[20] C. Orellana-Tavra, M. Köppen, A. Li, N. Stock, D. Fairen-Jimenez, Biocompatible, crystalline, and amorphous bismuth-based metal-organic frameworks for drug delivery, ACS Appl. Mater. Interfaces. 12 (2020) 5633–5641, https://doi.org/10.1021/acsami.9b21692.

[21] M. Nazari, M. Rubio-Martinez, G. Tobias, J.P. Barrio, R. Babarao, F. Nazari, K. Konstas, B.W. Muir, S.F. Collins, A.J. Hill, M.C. Duke, M.R. Hill, Metal-organic-framework-coated optical fibers as light-triggered drug delivery vehicles, Adv. Funct. Mater. 26 (2016) 3244–3249, https://doi.org/10.1002/adfm.201505260.

[22] K. Xing, R. Fan, F. Wang, H. Nie, X. Du, S. Gai, P. Wang, Y. Yang, Dual-stimulus-triggered programmable drug release and luminescent ratiometric pH sensing from chemically stable biocompatible zinc metal-organic framework, ACS Appl. Mater. Interfaces. 10 (2018) 22746–22756, https://doi.org/10.1021/acsami.8b06270.

[23] B.E. Souza, L. Donà, K. Titov, P. Bruzzese, Z. Zeng, Y. Zhang, A.S. Babal, A. F. Möslein, M.D. Frogley, M. Wolna, G. Cinque, B. Civalleri, J.-C. Tan, Elucidating the drug release from metal-organic framework nanocomposites via in situ synchrotron microspectroscopy and theoretical modeling, ACS Appl. Mater. Interfaces. 12 (2020) 5147–5156, https://doi.org/10.1021/acsami.9b21321.

[24] I. Abánades Lázaro, C.J.R. Wells, R.S. Forgan, Multivariate modulation of the Zr MOF UiO-66 for defect-controlled combination anticancer drug delivery, Angew. Chemie. 132 (2020) 5249–5255, https://doi.org/10.1002/ange.201915848.

[25] L. Zhang, Y.-F. Li, S. Yuan, S. Zhang, H. Zheng, J. Liu, P. Sun, Y. Gu, H. Kurihara, R.-R. He, H. Chen, Bioactivity focus of α-cyano-4-hydroxycinnamic acid (CHCA) leads to effective multifunctional aldose reductase inhibitors, Sci. Rep. 6 (2016) 24942, https://doi.org/10.1038/srep24942.

[26] X. Li, M. Porcino, J. Qiu, D. Constantin, C. Martineau-Corcos, R. Gref, Doxorubicin-loaded metal-organic frameworks nanoparticles with engineered cyclodextrin coatings: insights on drug location by solid state NMR spectroscopy, Nanomaterials. 11 (2021) 945, https://doi.org/10.3390/nano11040945.

[27] D. Chen, D. Yang, C.A. Dougherty, W. Lu, H. Wu, X. He, T. Cai, M.E. Van Dort, B. D. Ross, H. Hong, *In vivo* targeting and positron emission tomography imaging of tumor with intrinsically radioactive metal-organic frameworks nanomaterials, ACS Nano. 11 (2017) 4315–4327, https://doi.org/10.1021/acsnano.7b01530.

[28] X. Zhao, S. Liu, C. Hu, Y. Liu, M. Pang, J. Lin, Controllable synthesis of monodispersed NU-1000 drug carrier for chemotherapy, ACS Appl. Bio Mater. 2 (2019) 4436–4441, https://doi.org/10.1021/acsabm.9b00621.

[29] H. Zheng, Y. Zhang, L. Liu, W. Wan, P. Guo, A.M. Nyström, X. Zou, One-pot synthesis of metal-organic frameworks with encapsulated target molecules and their applications for controlled drug delivery, J. Am. Chem. Soc. 138 (2016) 962–968, https://doi.org/10.1021/jacs.5b11720.

[30] S. Rojas, A. Arenas-Vivo, P. Horcajada, Metal-organic frameworks: a novel platform for combined advanced therapies, Coord. Chem. Rev. 388 (2019) 202–226, https://doi.org/10.1016/j.ccr.2019.02.032.

[31] F. Hao, Z.-Y. Yan, X.-P. Yan, Recent advances in research on the effect of physicochemical properties on the cytotoxicity of metal–organic frameworks, Small Sci. 2 (2022) 2200044, https://doi.org/10.1002/smsc.202200044.

[32] P.J. Jodłowski, K. Dymek, G. Kurowski, J. Jaśkowska, W. Bury, M. Pander, S. Wnorowska, K. Targowska-Duda, W. Piskorz, A. Wnorowski, A. Boguszewska-Czubara, Zirconium-based metal–organic frameworks as acriflavine cargos in the battle against coronaviruses—a theoretical and experimental approach, ACS Appl. Mater. Interfaces. 14 (2022) 28615–28627, https://doi.org/10.1021/acsami.2c06420.

[33] P.J. Jodłowski, K. Dymek, G. Kurowski, K. Hyjek, A. Boguszewska-Czubara, B. Budzyńska, A. Pajdak, Ł. Kuterasiński, W. Piskorz, P. Jeleń, M. Sitarz, In vivo and in vitro studies of efficient mephedrone adsorption over zirconium-based metal-organic frameworks corroborated by DFT+D modeling, Microporous Mesoporous Mater. 359 (2023), 112647, https://doi.org/10.1016/j.micromeso.2023.112647.

[34] K. Hyjek, P. Jodłowski, Metal-organic frameworks for efficient drug adsorption and delivery, Sci. Radices. 2 (2023) 118–189, https://doi.org/10.58332/scirad2023v2i2a03.

[35] S.B. Raut, J.J. Canales, M. Ravindran, R. Eri, D.M. Benedek, R.J. Ursano, L. R. Johnson, Effects of propranolol on the modification of trauma memory reconsolidation in PTSD patients: a systematic review and meta-analysis, J. Psychiatr. Res. 150 (2022) 246–256, https://doi.org/10.1016/j.jpsychires.2022.03.045.

[36] J.D. Nguyen, S.M. Aarde, M. Cole, S.A. Vandewater, Y. Grant, M.A. Taffe, Locomotor stimulant and rewarding effects of inhaling methamphetamine, MDPV, and mephedrone via electronic cigarette-type technology, Neuropsychopharmacology. 41 (2016) 2759–2771, https://doi.org/10.1038/npp.2016.88.

[37] E. Papaseit, C. Pérez-Mañá, J.-A. Mateus, M. Pujadas, F. Fonseca, M. Torrens, E. Olesti, R. de la Torre, M. Farré, Human pharmacology of mephedrone in comparison with MDMA, Neuropsychopharmacology. 41 (2016) 2704–2713, https://doi.org/10.1038/npp.2016.75.
[38] J.H. Cavka, S. Jakobsen, U. Olsbye, N. Guillou, C. Lamberti, S. Bordiga, K. P. Lillerud, A new zirconium inorganic building brick forming metal organic frameworks with exceptional stability, J. Am. Chem. Soc. 130 (2008) 13850–13851, https://doi.org/10.1021/ja8057953.
[39] S. Dai, C. Simms, I. Dovgaliuk, G. Patriarche, A. Tissot, T.N. Parac-Vogt, C. Serre, Monodispersed MOF-808 nanocrystals synthesized via a scalable room-temperature approach for efficient heterogeneous peptide bond hydrolysis, Chem. Mater. 33 (2021) 7057–7066, https://doi.org/10.1021/acs.chemmater.1c02174.
[40] T.C. Wang, N.A. Vermeulen, I.S. Kim, A.B.F. Martinson, J.F. Stoddart, J.T. Hupp, O. K. Farha, Scalable synthesis and post-modification of a mesoporous metal-organic framework called NU-1000, Nat. Protoc. 11 (2016) 149–162, https://doi.org/10.1038/nprot.2016.001.
[41] E. Kozioł, K. Skalicka-Woźniak, A. Michalak, K. Kaszubska, B. Budzyńska, Xanthotoxin reverses Parkinson's disease-like symptoms in zebrafish larvae and mice models: a comparative study, Pharmacol. Reports. 73 (2021) 122–129, https://doi.org/10.1007/s43440-020-00136-9.
[42] K. Dymek, G. Kurowski, Ł. Kuterasiński, R. Jędrzejczyk, M. Szumera, M. Sitarz, A. Pajdak, Ł. Kurach, A. Boguszewska-Czubara, P.J. Jodłowski, In search of effective UiO-66 metal-organic frameworks for artificial kidney application, ACS Appl. Mater. Interfaces. 13 (2021) 45149–45160, https://doi.org/10.1021/acsami.1c05972.
[43] J.E. Efome, D. Rana, T. Matsuura, C.Q. Lan, Insight studies on metal-organic framework nanofibrous membrane adsorption and activation for heavy metal ions removal from aqueous solution, ACS Appl. Mater. Interfaces. 10 (2018) 18619–18629, https://doi.org/10.1021/acsami.8b01454.
[44] Y. Hong, J. Peng, Z. Sun, Z. Yu, A. Wang, Y. Wang, Y.-Y. Liu, F. Xu, L.-X. Sun, Transition metal oxodiperoxo complex modified metal-organic frameworks as catalysts for the selective oxidation of cyclohexane, Materials. 13 (2020) 829, https://doi.org/10.3390/ma13040829.
[45] G.C. Shearer, S. Chavan, S. Bordiga, S. Svelle, U. Olsbye, K.P. Lillerud, Defect engineering: tuning the porosity and composition of the metal-organic framework UiO-66 via modulated synthesis, Chem. Mater. 28 (2016) 3749–3761, https://doi.org/10.1021/acs.chemmater.6b00602.
[46] J.E. Mondloch, M.J. Katz, N. Planas, D. Semrouni, L. Gagliardi, J.T. Hupp, O. K. Farha, Are Zr6-based MOFs water stable? Linker hydrolysis vs. capillary-force-driven channel collapse, Chem. Commun. 50 (2014) 8944–8946, https://doi.org/10.1039/c4cc02401j.
[47] I. Langmuir, The adsorption of gases on plane surfaces of glass, mica and platinum, J. Am. Chem. Soc. 40 (1918) 1361–1403, https://doi.org/10.1021/ja02242a004.
[48] S. Brunauer, The Adsorption of Gases and Vapors: physical adsorption, Princeton University Press, 1943.
[49] B. Ambrozini, P. Cervini, É.T.G. Cavalheiro, Thermal behavior of the β-blocker propranolol, J. Therm. Anal. Calorim. 123 (2016) 1013–1017, https://doi.org/10.1007/s10973-015-5118-7.
[50] J.B.M. Fernandes, M.T. Celestino, M.I.B. Tavares, Z.M.F. Freitas, E.P. Dos Santos, E. Ricci Júnior, M.S.S.B. Monteiro, The development and characterization of propranolol tablets using tapioca starch as excipient, An. Acad. Bras. Cienc. 91 (2019), e20180094, https://doi.org/10.1590/0001-3765201920180009.
[51] K. Chaturvedi, S. Umadevi, S. Vaghani, Floating matrix dosage form for propranolol hydrochloride based on gas formation technique: development and *in vitro* evaluation, Sci. Pharm. 78 (2010) 927–940, https://doi.org/10.3797/scipharm.0909-02.
[52] A.M.J. Newton, S.M. Rani, K. Sukhjinder, Fabrication and evaluation of fast disintegrating oral hybrid films of propranolol hydrochloride by using pectin and synthetic polymers, J. Dev. Drugs. 5 (2016) 1000157, https://doi.org/10.4172/2329-6631.1000157.
[53] C.A. Clark, K.N. Heck, C.D. Powell, M.S. Wong, Highly defective UiO-66 materials for the adsorptive removal of perfluorooctanesulfonate, ACS Sustain. Chem. Eng. 7 (2019) 6619–6628, https://doi.org/10.1021/acssuschemeng.8b05572.
[54] H.-Q. Zheng, Y.-N. Zeng, J. Chen, R.-G. Lin, W.-E. Zhuang, R. Cao, Z.-J. Lin, Zr-based metal-organic frameworks with intrinsic peroxidase-like activity for ultradeep oxidative desulfurization: mechanism of H_2O_2 decomposition, Inorg. Chem. 58 (2019) 6983–6992, https://doi.org/10.1021/acs.inorgchem.9b00604.
[55] A. Farcaș, C. Iacoviță, E. Vințeler, V. Chiș, R. Știufiuc, C.M. Lucaciu, The influence of molecular structure modifications on vibrational properties of some beta blockers: a combined Raman and DFT study, J. Spectrosc. 2016 (2016) 1–9, https://doi.org/10.1155/2016/3137140.
[56] C. Atzori, G.C. Shearer, L. Maschio, B. Civalleri, F. Bonino, C. Lamberti, S. Svelle, K. P. Lillerud, S. Bordiga, Effect of benzoic acid as a modulator in the structure of UiO-66: an experimental and computational study, J. Phys. Chem. c. 121 (2017) 9312–9324, https://doi.org/10.1021/acs.jpcc.7b00483.
[57] M. Sen Bishwas, M. Malik, P. Poddar, Raman spectroscopy-based sensitive, fast and reversible vapour phase detection of explosives adsorbed on metal-organic frameworks UiO-67, New J. Chem. 45 (2021) 7145–7153, https://doi.org/10.1039/d0nj04915h.
[58] H. Hernawan, S. Nurhayati, K. Nisa, A.W. Indrianingsih, C. Darsih, M. Kismurtono, Formulation and *in vitro* study of propranolol hydrochloride controlled release from carboxymethyl chitosan-based matrix tablets, Indones. J. Chem. 13 (2013) 242–247, https://doi.org/10.22146/ijc.2128.
[59] H. Dong, G.-X. Yang, X. Zhang, X.-B. Meng, J.-L. Sheng, X.-J. Sun, Y.-J. Feng, F.-M. Zhang, Folic acid functionalized zirconium-based metal–organic frameworks as drug carriers for active tumor-targeted drug delivery, Chem. Eur. J. 24 (2018) 17148, https://doi.org/10.1002/chem.201804153.
[60] M.de J. Velásquez-Hernández, R. Ricco, F. Carraro, F.T. Limpoco, M. Linares-Moreau, E. Leitner, H. Wiltsche, J. Rattenberger, H. Schröttner, P. Frühwirt, E. M. Stadler, G. Gescheidt, H. Amenitsch, C.J. Doonan, P. Falcaro, Degradation of ZIF-8 in phosphate buffered saline media, CrystEngComm. 21 (2019) 4538–4544, https://doi.org/10.1039/c9ce00757a.
[61] H. Bunzen, Chemical stability of metal-organic frameworks for applications in drug delivery, ChemNanoMat. 7 (2021) 998, https://doi.org/10.1002/cnma.202100226.
[62] R. Ettlinger, U. Lächelt, R. Gref, P. Horcajada, T. Lammers, C. Serre, P. Couvreur, R. E. Morris, S. Wuttke, Toxicity of metal–organic framework nanoparticles: from essential analyses to potential applications, Chem. Soc. Rev. 51 (2022) 464–484, https://doi.org/10.1039/D1CS00918D.
[63] A. Ruyra, A. Yazdi, J. Espín, A. Carné-Sánchez, N. Roher, J. Lorenzo, I. Imaz, D. Maspoch, Synthesis, culture medium stability, and in vitro and in vivo zebrafish embryo toxicity of metal-organic framework nanoparticles, Chem. Eur. J. 21 (2015) 2508–2518, https://doi.org/10.1002/chem.201405380.
[64] Y. Yang, H. Bao, Q. Chai, Z. Wang, Z. Sun, C. Fu, Z. Liu, Z. Liu, X. Meng, T. Liu, Toxicity, biodistribution and oxidative damage caused by zirconia nanoparticles after intravenous injection, Int. J. Nanomedicine. 14 (2019) 5175–5186, https://doi.org/10.2147/IJN.S197565.
[65] B.M. Jarai, Z. Stillman, L. Attia, G.E. Decker, E.D. Bloch, C.A. Fromen, Evaluating UiO-66 metal-organic framework nanoparticles as acid-sensitive carriers for pulmonary drug delivery applications, ACS Appl. Mater. Interfaces. 12 (2020) 38989–39004, https://doi.org/10.1021/acsami.0c10900.
[66] G. Kresse, J. Hafner, *Ab initio* molecular dynamics for open-shell transition metals, Phys. Rev. b. 48 (1993) 13115–13118, https://doi.org/10.1103/physrevb.48.13115.
[67] H.J.C. Berendsen, D. van der Spoel, R. van Drunen, GROMACS: a message-passing parallel molecular dynamics implementation, Comput. Phys. Commun. 91 (1995) 43–56, https://doi.org/10.1016/0010-4655(95)00042-E.
[68] M.J. Abraham, T. Murtola, R. Schulz, S. Páll, J.C. Smith, B. Hess, E. Lindahl, GROMACS: high performance molecular simulations through multi-level parallelism from laptops to supercomputers, SoftwareX. 1–2 (2015) 19–25, https://doi.org/10.1016/j.softx.2015.06.001.